Variational moment solutions to the Grad–Shafranov equation

L. L. Lao, S. P. Hirshman, and R. M. Wieland

Citation: The Physics of Fluids **24**, 1431 (1981); doi: 10.1063/1.863562
View online: https://doi.org/10.1063/1.863562
View Table of Contents: https://aip.scitation.org/toc/pfl/24/8
Published by the American Institute of Physics

Variational moment solutions to the Grad–Shafranov equation

L. L. Lao, S. P. Hirshman, and R. M. Wieland

Oak Ridge National Laboratory, Oak Ridge, Tennessee 37830
(Received 17 November 1980; accepted 23 April 1981)

A variational method is developed to find approximate solutions to the Grad–Shafranov equation. The surfaces of the constant poloidal magnetic flux $\psi(R, Z)$ are obtained by solving a few ordinary differential equations, which are moments of the Grad–Shafranov equation, for the Fourier amplitudes of the inverse mapping $R(\psi, \theta)$ and $Z(\psi, \theta)$. Analytic properties and solutions of the moment equations are considered. Specific calculations using the Impurity Study Experiment (ISX-B) and the Engineering Test Facility (ETF)/International Tokamak Reactor (INTOR) geometries are performed numerically, and the results agree well with those calculated using standard two-dimensional equilibrium codes. The main advantage of the variational moment method is that it significantly reduces the computational time required to determine two-dimensional equilibria without sacrificing accuracy.

I. INTRODUCTION

For transport simulations of high beta (poloidal betas on the order of the aspect ratio), noncircular tokamak plasmas, it is important to have a computationally fast, yet sufficiently accurate, method for determining the flux surface geometry. Repeatedly solving the two-dimensional Grad–Shafranov equation for the evolving flux surface geometry can significantly increase the computer time and storage requirements of a transport code. In this paper, a variational method is developed to find approximate solutions to the Grad–Shafranov equation that are computationally efficient. The flux surface coordinates (R, Z) are expanded in Fourier series in a poloidal angle θ. Through the use of the variational method, the Fourier amplitudes of R and Z are obtained by solving a set of coupled ordinary differential equations, which are moments of the Grad–Shafranov equation. The approximation for the flux surface geometry obtained in this way is sufficiently accurate for transport simulations and may also be used to evaluate magnetohydrodynamic stability criteria.

In Sec. II, the coordinate system and the variational principle are introduced. The moment equations for the Fourier coefficients of the inverse mapping are derived in Sec. III. In Sec. IV, some analytic properties and solutions of the moment equations are considered. Finally, in Sec. V, comparisons of the approximate moment solutions with two-dimensional calculations are presented, and a brief discussion of the numerical method used to solve the moment equations is given.

II. ANALYTIC FORMULATION OF THE INVERSE EQUILIBRIUM PROBLEM

A. Coordinate transformation

In considering a two-dimensional axisymmetric toroidal system with nested magnetic surfaces, it is convenient to transform the cylindrical coordinates (R, Z) to the flux surface representation (ρ, θ), where $\rho = \rho(\psi)$ is a flux surface label, θ is a poloidal angle that increases by 2π the short way around the torus, and ψ is the poloidal magnetic flux enclosed between the flux surface $\rho(\psi)$ and the axis of symmetry (Fig. 1). The angle θ is arbitrary, except that the Jacobian of the transformation is finite. Assuming that the flux surfaces possess up-down symmetry $[Z(\rho, \theta) = -Z(\rho, -\theta)]$, it is possible to represent the coordinate transformation as a Fourier series in θ:

$$R(\rho, \theta) = \sum_{n=0}^{\infty} R_n(\rho) \cos n\theta , \tag{1}$$

$$Z(\rho, \theta) = \sum_{n=1}^{\infty} Z_n(\rho) \sin n\theta . \tag{2}$$

The amplitudes $R_0(\rho)$, $R_1(\rho)$, and $Z_1(\rho)$ describe the shift, the minor radius, and the ellipticity of the flux surfaces, respectively, whereas the amplitudes $R_2(\rho)$ and $Z_2(\rho)$ describe the triangularity of the flux surfaces. For example, if only the amplitudes $R_0(\rho)$, $R_1(\rho)$, and $Z_1(\rho)$ are retained, the flux surfaces are shifted ellipses. These are illustrated in Fig. 1(a). The effects of triangularity (R_2, Z_2) and quadrangularity (R_3, Z_3) are shown in Figs. 1(b–c), respectively. Analyses of high beta ($\beta_p \sim R_0/a$) equilibria, such as those describing the Impurity Study Experiment (ISX-B) and the Engineering Test Facility (ETF)/International Tokamak Reactor (INTOR), show that the choice of a convenient poloidal angle θ yields a rapidly converging Fourier series[1] for the flux surface coordinates $R(\rho, \theta)$ and $Z(\rho, \theta)$. It is found, in practice, that a few amplitudes [$n \leq 3$ in Eqs. (1) and (2)] are sufficient to describe the equilibrium geometry even for a high beta, strongly D-shaped plasma. Thus, the problem of finding two-dimensional magnetohydrodynamic equilibria may be reduced to that of solving a few coupled ordinary differential equations for the Fourier amplitudes R_n and Z_n. Equations (1) and (2) are reminiscent of the pioneering work by Greene *et al.*,[2] who treated the poloidal harmonic couplings occurring in the low beta ($\beta_p \sim 1$) ordering in toroidal geometry. The low beta result in Ref. 2 follows as a limit of the present calculations, which are valid for arbitrary beta.

B. Variational principle

The Fourier series for R and Z may be substituted into the Grad–Shafranov equation expressed in (ρ, θ) coordinates (the inverse of the Grad-Shafranov equa-

 0031-9171/81/081431-11$00.90

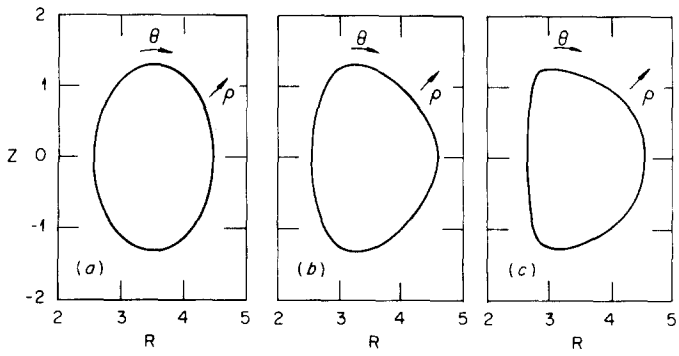

FIG. 1. Flux surface geometry: (a) $R=3.5-\cos\theta$, $Z=1.3\sin\theta$; (b) $R=3.5-\cos\theta+0.1\cos2\theta$, $Z=1.3\sin\theta+0.13\sin2\theta$; (c) $R=3.5-\cos\theta+0.1\cos2\theta+0.05\cos3\theta$, $Z=1.3\sin\theta+0.13\sin2\theta+0.065\sin3\theta$.

tion) to yield an infinite system of coupled ordinary differential equations for the expansion coefficients.[2] In practice, only a finite number N of amplitude functions will be retained to obtain an approximate solution for the flux surface geometry. Since the inverse Grad–Shafranov equation is nonlinear in R and Z, the resulting harmonic coupling generally yields (for finite N) more equations than the number of Fourier amplitudes. Therefore, a method must be determined for selecting the appropriate linear combination of these equations that will yield the best approximate solution. A variational principle will now be introduced from which the "optimum" ordinary differential equations for the Fourier amplitudes of the inverse mapping may be obtained. A related approach has been developed by Hait[3] and applied to the particular case of shifted elliptical flux surfaces.

Consider the Grad–Shafranov equation

$$\Delta^*\psi(R,Z)=-(8\pi^2R/c)J_\phi\,, \tag{3}$$

where J_ϕ is the toroidal component of the current density

$$J_\phi=2\pi cR[p'(\psi)+FF'(\psi)/\pi c^2R^2]\,, \tag{4}$$

F is the poloidal current enclosed between the axis of symmetry and the magnetic surface of interest, and

$$\Delta^*\psi(R,Z)\equiv R^2\nabla\cdot\left(\frac{\nabla\psi}{R^2}\right)=\frac{\partial^2\psi}{\partial R^2}-\frac{1}{R}\frac{\partial\psi}{\partial R}+\frac{\partial^2\psi}{\partial Z^2}\,. \tag{5}$$

Throughout this paper, the prime superscript on a function denotes differentiation with respect to its argument; $p'(\psi)=dp/d\psi$, $p'(\rho)=dp/d\rho$, etc.

Now consider the volume integral

$$Q=\int_V dR\,dZ\,L(\psi,\psi_R,\psi_Z,R)\,, \tag{6}$$

where $\psi_R=\partial\psi/\partial R$, $\psi_Z=\partial\psi/\partial Z$, L is the Lagrangian

$$L=R\left(\frac{B_p^2}{8\pi}-\frac{B_t^2}{8\pi}-p(\psi)\right), \tag{7}$$

and the integration is over the entire plasma volume V.

Here, B_p and B_t are the poloidal and the toroidal magnetic field components, respectively

$$B_p=|\nabla\psi|/2\pi R\,, \tag{8}$$

$$B_t=2F(\psi)/cR\,. \tag{9}$$

Using the fact that the operator $R^{-2}\Delta^*$ is self-adjoint, it may be shown that Q is stationary with respect to variations of ψ, although subject to the constraint $\delta\psi$ (boundary) = 0, for ψ satisfying the Grad–Shafranov equation. Conversely, the Euler equation

$$\frac{\partial L}{\partial\psi}-\frac{\partial}{\partial R}\frac{\partial L}{\partial\psi_R}-\frac{\partial}{\partial Z}\frac{\partial L}{\partial\psi_Z}=0 \tag{10}$$

reproduces the Grad–Shafranov equation. Note that $B_p^2/8\pi\propto|\nabla\psi|^2$ plays the role of kinetic energy in Eq. (7) and that $B_t^2/8\pi+p(\psi)$ is the effective potential energy. Indeed, the Hamiltonian corresponding to the Lagrangian L is proportional to the total energy in the equilibrium system.

Now consider the transformation in Eq. (6) of the independent (integration) variables (R,Z) to (ρ,θ) coordinates

$$Q=\int_0^a\int_0^{2\pi}d\rho\,d\theta\,\tilde L(R,R_\rho,R_\theta,Z_\rho,Z_\theta,\psi,\psi_\rho)\,. \tag{11}$$

Here, $\rho=a$ denotes the outermost flux surface and the subscripts ρ and θ denote differentiation with respect to these variables. The transformed Lagrangian is

$$\tilde L\equiv\sqrt{g}\left(\frac{1}{32\pi^3}\frac{g_{\theta\theta}}{g}[\psi'(\rho)]^2-\frac{F^2(\psi)}{2\pi c^2R^2}-p(\psi)\right), \tag{12}$$

where $\sqrt{g}$ is the (three-dimensional) Jacobian of the transformation from (R,ϕ,Z) to (ρ,θ,ϕ) coordinates (ϕ is the ignorable toroidal angle)

$$\sqrt{g}=R\tau\,, \tag{13}$$

$$\tau=R_\theta Z_\rho-R_\rho Z_\theta\,, \tag{14}$$

and $g_{\mu\nu}$, for $(\mu,\nu)\in(\rho,\theta)$, are the elements of the metric tensor

$$g_{\mu\nu}=R_\mu R_\nu+Z_\mu Z_\nu\,, \tag{15}$$

and

$$g_{\phi\phi}=R^2\,. \tag{16}$$

All other metric elements are zero. In the representation of Q given by Eq. (11), the quantities R, Z, and ψ are interpreted as dependent variables.

Since Q is a scalar, its value must be independent of the particular coordinate representation used in its evaluation. Thus, the form for Q given in Eq. (11) must be stationary with respect to variations of the dependent variables R and Z, which are subject to the fixed boundary constraints δR (boundary) = 0 or δZ(boundary) = 0. The variation of Q with respect to these variables yields

$$\delta Q_R=\int_0^a\int_0^{2\pi}d\rho\,d\theta\,\delta R\left(\frac{\partial\tilde L}{\partial R}-\frac{\partial}{\partial\rho}\frac{\partial\tilde L}{\partial R_\rho}-\frac{\partial}{\partial\theta}\frac{\partial\tilde L}{\partial R_\theta}\right)$$

$$= -\int_0^a\int_0^{2\pi} d\rho\, d\theta\, \delta R\, R Z_\theta \hat{G}\,, \tag{17}$$

and

$$\delta Q_Z = \int_0^a\int_0^{2\pi} d\rho\, d\theta\, \delta Z\left(-\frac{\partial}{\partial\rho}\frac{\partial\tilde{L}}{\partial Z_\rho} - \frac{\partial}{\partial\theta}\frac{\partial\tilde{L}}{\partial Z_\theta}\right)$$

$$= \int_0^a\int_0^{2\pi} d\rho\, d\theta\, \delta Z\, R R_\theta \hat{G}\,, \tag{18}$$

where

$$\hat{G} = \frac{\psi'(\rho)}{16\pi^3\sqrt{g}}\left[\frac{\partial}{\partial\rho}\left(\frac{g_{\theta\theta}}{\sqrt{g}}\psi'(\rho)\right) - \frac{\partial}{\partial\theta}\left(\frac{g_{\rho\theta}}{\sqrt{g}}\psi'(\rho)\right)\right]$$

$$+ p'(\rho) + \frac{FF'(\rho)}{\pi c^2 R^2}\,. \tag{19}$$

Note that $\hat{G} = \psi'(\rho)(16\pi^3R^2)^{-1}(\Delta^*\psi + 8\pi^2 R J_\phi/c)$ is proportional to the equilibrium operator in Eq. (3) expressed in (ρ,θ) coordinates. It follows that Q is stationary if $R(\rho,\theta)$ or $Z(\rho,\theta)$ satisfies the inverse Grad–Shafranov equation[2,4]

$$\hat{G} = 0\,, \tag{20}$$

and that, conversely, the Euler equation

$$\frac{\partial\tilde{L}}{\partial R} - \frac{\partial}{\partial\rho}\frac{\partial\tilde{L}}{\partial R_\rho} - \frac{\partial}{\partial\theta}\frac{\partial\tilde{L}}{\partial R_\theta} = 0\,, \tag{21}$$

or

$$\frac{\partial}{\partial\rho}\frac{\partial\tilde{L}}{\partial Z_\rho} + \frac{\partial}{\partial\theta}\frac{\partial\tilde{L}}{\partial Z_\theta} = 0\,, \tag{22}$$

reproduces the inverse Grad–Shafranov equation. The fact that varying either R or Z yields the same Eq. (20) expresses the arbitrariness of the poloidal angle θ. For example, if θ is chosen such that the (ρ,θ) coordinates are orthogonal, Eq. (20) [together with the orthogonality condition $\nabla\rho\cdot\nabla\theta \equiv -\tau^{-2}(R_\rho R_\theta + Z_\rho Z_\theta) = 0$] yield the set of inverse equilibrium equations used by Vabishchevich *et al.*[4]

Thus, the variational principle derived here may be summarized as follows: In a two-dimensional axisymmetric toroidal system, the equilibrium flux surface geometry described by $\psi(R,Z)$, or parametrically by $R(\rho,\theta)$ and $Z(\rho,\theta)$, is such that the volume integral Q defined in Eq. (6) is stationary.

III. MOMENT EQUATIONS FOR THE INVERSE MAPPING

A. Determination of the Fourier expansion coefficients

The variational principle just developed provides a well-defined algorithm to calculate the Fourier amplitudes $R_n(\rho)$ and $Z_n(\rho)$, when n is finite, by requiring that Q be stationary with respect to the variations of these amplitudes. Varying Q with respect to a particular amplitude $R_n(\rho)$ or $Z_n(\rho)$ yields the Euler equation describing $R_n(\rho)$ or $Z_n(\rho)$:

$$\left\langle\frac{\partial\tilde{L}}{\partial R_n} - \frac{\partial}{\partial\rho}\frac{\partial\tilde{L}}{\partial R_n'}\right\rangle = 0;\quad n = 0, 1, \ldots\,, \tag{23}$$

or

$$\left\langle\frac{\partial\tilde{L}}{\partial Z_n} - \frac{\partial}{\partial\rho}\frac{\partial\tilde{L}}{\partial Z_n'}\right\rangle = 0;\quad n = 1, 2, \ldots\,, \tag{24}$$

where the prime denotes differentiation with respect to ρ, and $\langle A\rangle$ is the poloidal angle averaging operator defined for any scalar A as

$$\langle A\rangle = \int_0^{2\pi}\frac{d\theta}{2\pi}A\,. \tag{25}$$

This operator is related to the flux surface averaging operator $\langle A\rangle_f$:

$$\langle A\rangle_f = \langle\sqrt{g}A\rangle/\langle\sqrt{g}\rangle\,. \tag{26}$$

Although $\tilde{L}$, defined in Eq. (12), does not depend on the coordinate Z, it does depend on the amplitudes Z_n through Z_θ. This explains the appearance of the first term in Eq. (24).

Equations (23) and (24) comprise a system of coupled, second-order, nonlinear ordinary differential equations in ρ for the Fourier amplitudes R_n and Z_n. The relationship of this system to the inverse Grad–Shafranov equation (20) can be elucidated by considering a particular representation for the poloidal angle θ. For example, representing the inverse mapping as a truncated Fourier series

$$R(\rho,\theta) = \sum_{n=0}^{n_R} R_n(\rho)\cos n\theta\,, \tag{27}$$

and

$$Z(\rho,\theta) = \sum_{n=1}^{n_Z} Z_n(\rho)\sin n\theta\,, \tag{28}$$

and varying all the amplitudes independently, the Euler equations (23) and (24) yield

$$\langle M_{R_n}\hat{G}\rangle = 0;\quad n = 0, 1, \ldots, n_R\,, \tag{29}$$

$$\langle M_{Z_n}\hat{G}\rangle = 0;\quad n = 1, \ldots, n_Z\,, \tag{30}$$

where

$$M_{R_n} = R Z_\theta \cos n\theta; \tag{31}$$

and

$$M_{Z_n} = R R_\theta \sin n\theta; \tag{32}$$

Alternatively, using the convenient Fourier representation[1] (cf, the Appendix)

$$R(\rho,\theta) = R_0(\rho) - R_1(\rho)\cos\theta + \sum_{n=2}^{n_R} R_n(\rho)\cos n\theta\,, \tag{33}$$

$$Z(\rho,\theta) = E(\rho)\sum_{n=1}^{n_R} R_n(\rho)\sin n\theta\,, \tag{34}$$

where the constraint $Z_n = E R_n$ was imposed, the equations for $E(\rho)$ and $R_n(\rho)$ are, respectively:

$$\left\langle\left(\sum_{n=1}^{n_R} R_n M_{Z_n}\right)\hat{G}\right\rangle = 0\,, \tag{35}$$

$$\langle M_{R_0}\hat{G}\rangle = 0\,, \tag{36}$$

$$\langle(E M_{Z_1} + M_{R_1})\hat{G}\rangle = 0\,, \tag{37}$$

$$\langle(E M_{Z_n} - M_{R_n})\hat{G}\rangle = 0;\quad n = 2, \ldots, n_R\,. \tag{38}$$

Thus, the Fourier expansion coefficients R_n and Z_n are determined by *moments* of the inverse equilibrium equation with respect to the weighting functions M_{Rn} and M_{Zn} or their linear combinations. In the limit $(n_R, n_Z) \to \infty$, either of these sets of weighting functions can be used as a complete set of poloidal basis functions for expanding an arbitrary, even function of θ. (The assumption of up-down symmetry of the flux surfaces restricts the class of functions that can be represented in terms of M_{Rn} or M_{Zn} to those even in θ, but this restriction can be readily relaxed.)

The present variational moment method contrasts with the moment method of Zakharov and Shafranov[5,6] in which the class of homogeneous solutions $H_n(R, Z)$ of the Δ^* operator, which are polynomials in (R, Z), were used as weighting functions to obtain a system of coupled ordinary differential equations $\langle H_n(R,Z)\hat{G}\rangle_f = 0$. This latter method is not based on a variational principle and is, therefore, arbitrary in its specification of which H_n, or combination of H_n's, should be used for a given finite-term expansion of the inverse mapping. Typically, the lowest order H_n's are used for convenience although these do not correspond to the variational weighting functions M_{Rn} or M_{Zn}. However, in practical applications, when the amplitudes of the high harmonics R_n and Z_n $(n \geq 2)$ are small compared with R_1, combinations of the variational moment equations (29) and (30) can be found that approximately reproduce the low order, homogeneous moment equations. In this way, the variational moment method justifies the otherwise arbitrary homogeneous moment method and establishes the conditions under which the latter method might fail.

B. Determination of the flux surface label

There are two ways to obtain the relationship between the flux surface coordinate ρ and the actual poloidal flux ψ. One of the Fourier amplitudes (R_1, for example[5]) may be used as the flux surface label. Then, Q cannot be varied with respect to that particular amplitude; rather, the variation of Q with respect to ψ can be used to obtain the surface averaged pressure balance equation

$$\langle \sqrt{g}\,\hat{G}\rangle = 0 . \tag{39}$$

In general, if neither the amplitudes R_n or Z_n nor ψ is used as the flux surface label, the average pressure balance equation (39) may be expressed as a linear combination of the moment equations (29) and (30) or (35)–(38), and it is therefore not an independent equation. In this case, the poloidal flux $\psi(\rho)$ is found from the equation defining the flux surface label ρ, which must be independently specified.

C. Alternate form of the moment equations

Generally, the flux function $F(\psi)$ varies only weakly across the plasma cross section $|F(\rho=a) - F(0)|/|F(0)| \sim \beta_t \ll 1$, where β_t is the toroidal beta. The flux surface geometry is, therefore, sensitive to small inaccuracies in the prescription of the $F(\psi)$ profile. For numerical convenience, it has been found useful to eliminate $F(\psi)$ in the moment equations in terms of the total toroidal current enclosed by a flux surface $I(\rho) \equiv \int_0^\rho \mathbf{J}\cdot\nabla\phi\, dV$. Typically, $I(\rho)$ vanishes at the magnetic axis $\rho = 0$ and increases monotonically to the value I_0 at the plasma edge, where I_0 is the total toroidal plasma current; $I(\rho)$ may be related to the poloidal magnetic field through the surface average of the toroidal component of Ampere's law [Eq. (3)]:

$$\psi'(\rho) = \frac{-4\pi}{c}\frac{I(\rho)}{\langle g_{\theta\theta}/\sqrt{g}\rangle} . \tag{40}$$

Furthermore, the surface averaged pressure balance equation (39) can be used to eliminate F in terms of I:

$$FF'(\psi) = \frac{c}{4\pi}\frac{\langle g_{\theta\theta}/\sqrt{g}\rangle}{\langle \sqrt{g}/g_{\phi\phi}\rangle I(\rho)}\left(\pi c^2\langle\sqrt{g}\rangle p'(\rho) + \frac{II'(\rho)}{\langle g_{\theta\theta}/\sqrt{g}\rangle}\right). \tag{41}$$

Substituting Eqs. (40) and (41) into the inverse equilibrium operator [Eq. (19)], the moment equations (29) and (30) or (35)–(38) are modified by replacing $\hat{G}(FF', \psi')$ with $\tilde{G}(I, I')$, where

$$\tilde{G} = \frac{I^2(\rho)}{\pi c^2\sqrt{g}\langle g_{\theta\theta}/\sqrt{g}\rangle}\left[\frac{\partial}{\partial\rho}\left(\frac{g_{\theta\theta}}{\sqrt{g}\langle g_{\theta\theta}/\sqrt{g}\rangle}\right) - \frac{\partial}{\partial\theta}\left(\frac{g_{\rho\theta}}{\sqrt{g}\langle g_{\theta\theta}/\sqrt{g}\rangle}\right)\right] + \frac{II'(\rho)}{\pi c^2\langle g_{\theta\theta}/\sqrt{g}\rangle}\left(\frac{g_{\theta\theta}}{g\langle g_{\theta\theta}/\sqrt{g}\rangle} - \frac{1}{g_{\phi\phi}\langle\sqrt{g}/g_{\phi\phi}\rangle}\right) + p'(\rho)\left(1 - \frac{\langle\sqrt{g}\rangle}{g_{\phi\phi}\langle\sqrt{g}/g_{\phi\phi}\rangle}\right). \tag{42}$$

In this form of the inverse operator, the constraint $I = I_0$ at the plasma boundary is readily imposed. Also, the average pressure balance $\langle\sqrt{g}\,\tilde{G}\rangle = 0$ is automatically satisfied.

Thus, given two "free" functions $p(\psi)$ and $F(\psi)$, or more conveniently $p(\rho)$ and $I(\rho)$, the moment equations (29) and (30) or (35)–(38) define a set of coupled ordinary differential equations that can be solved for the Fourier expansion coefficients $R_n(\rho)$ and $Z_n(\rho)$. In contrast to solving the Grad–Shafranov equation on a two-dimensional spatial grid, the moment solution immediately yields the magnetic surface geometry $\psi(R, Z) = \text{const}$. This eliminates the laborious procedure of reconstructing contour curves from a gridded $\psi(R, Z)$ solution.

IV. PROPERTIES OF THE MOMENT EQUATIONS

A. Analytic properties of the amplitudes near the magnetic axis

In this section, the behavior of the expansion coefficients of the inverse mapping in the vicinity of the magnetic axis $\psi = \psi_m$ is considered. The asymptotic properties of these amplitudes near the magnetic axis are required to obtain the global numerical solution of the moment equations derived in the previous section. The poloidal magnetic flux $\psi(R, Z)$ is assumed to be analytic at the magnetic axis, so that near the magnetic axis it can be represented by a power series in $Y \equiv R - R_m$ and Z:

$$\psi(R,Z) = \psi_m + \psi_{20}Y^2 + \psi_{02}Z^2 + \psi_{30}Y^3 + \psi_{12}YZ^2 + \dots . \tag{43}$$

Here, R_m is the major radius of the magnetic axis, ψ_m

$=\psi(R_m, 0)$, and the flux surfaces have up-down symmetry. Note that ψ has an extremum at the magnetic axis. Thus, the flux surfaces near the magnetic axis are concentric ellipses that can be conveniently represented as

$$R(\rho,\theta)=R_m-\rho\cos\theta+O(\rho^2)\,, \tag{44}$$

$$Z(\rho,\theta)=E_m\rho\sin\theta+O(\rho^2)\,, \tag{45}$$

where E_m is the ellipticity at the magnetic axis and the amplitude of the first harmonic of R was chosen as the flux surface label ρ. It follows from this choice of (ρ,θ) that at the magnetic axis $\rho=0$

$$R_n(0)=0;\quad n=2,3,\ldots\,, \tag{46}$$

$$Z_n(0)=0;\quad n=1,2,\ldots\,, \tag{47}$$

$$R_n'(0)=0;\quad n=0,2,3,\ldots\,, \tag{48}$$

$$Z_n'(0)=0;\quad n=2,3,\ldots\,, \tag{49}$$

where the prime denotes differentiation with respect to ρ. Now, consider the Fourier representation in Eqs. (33) and (34), of which Eqs. (44) and (45) are the lowest order terms in the ρ expansion. Equation (43) can be rewritten as

$$\psi_{20}Y^2+\psi_{02}Z^2=[\psi(\rho)-\psi_m]-\psi_{30}Y^3-\psi_{12}YZ^2+\ldots\,. \tag{50}$$

Expanding $\psi(\rho)-\psi_m$ in a power series in ρ and substituting the lower order Fourier representation of (R,Z) into the right-hand side of Eq. (50) yields

$$E(\rho)=E_m+E_2\rho^2+\ldots\,, \tag{51}$$

$$R_0(\rho)=R_m+R_{02}\rho^2+\ldots\,, \tag{52}$$

$$R_n(\rho)=\rho^n(R_{n0}+\ldots);\quad n=2,\ldots\,. \tag{53}$$

It follows from Eq. (51) that

$$E'(0)=0\,. \tag{54}$$

Alternatively, if the Fourier representation in Eqs. (27) and (28) is used and the poloidal angle θ is chosen such that $R_n\sim\rho^n$ (or $Z_n\sim\rho^n$), it can be shown that $Z_n\sim\rho^n$ (or $R_n\sim\rho^n$). Finally, substituting Eq. (43) for ψ into the Grad–Shafranov equation (3) and linearizing $p(\psi)$ and $F^2(\psi)$ yields

$$\psi(\rho)=\psi_m-\frac{8\pi^3E_m^2}{E_m^2+1}\left(R_m^2\frac{\partial p(0)}{\partial\psi}+\frac{1}{2\pi c^2}\frac{\partial F^2(0)}{\partial\psi}\right)\rho^2+O(\rho^4)\,. \tag{55}$$

It follows from Eq. (55) that

$$\psi'(0)=0\,. \tag{56}$$

Note that for numerical computations, it is more convenient to use R_1, the amplitude of the first harmonic of R, as the flux surface label ρ rather than the poloidal magnetic flux ψ, since $R_1'(\psi), Z_1'(\psi), R_3''(\psi), Z_3''(\psi)$, etc., are infinite at the magnetic axis. If the amplitudes of the high harmonics ($n\geq 3$) of R are small, R_1 is approximately equal to the minor radius of the flux surface on the plane $Z=0$.

B. Expansion of the moment equations

Generally, the θ integrals appearing in the coefficients of the amplitude equations cannot be evaluated analytically. The moment equations are nonlinear differential equations, which are also not amenable to analytic solutions. However, analytic calculations are possible near the magnetic axis or, for low beta plasmas, when the flux surface geometry $R(\rho,\theta)$ and $Z(\rho,\theta)$ can be approximated by the shifted ellipses

$$R(\rho,\theta)=R_m-\Delta(\rho)-\rho\cos\theta\,, \tag{57}$$

$$Z(\rho,\theta)=E(\rho)\rho\sin\theta\,. \tag{58}$$

Here, $\Delta(\rho)$ and $E(\rho)$ are the shift and the ellipticity of the flux surfaces, respectively. The moment equations determining $\Delta(\rho)$ and $E(\rho)$ are obtained from Eqs. (29) and (30):

$$\langle RZ_\theta\tilde{G}\rangle=0\,, \tag{59}$$

$$\langle RR_\theta\sin\theta\tilde{G}\rangle=0\,. \tag{60}$$

The analytic evaluation of the metric coefficients appearing in $\tilde{G}$ is possible for the inverse mapping given by Eqs. (57) and (58) if the variation of the ellipticity $E(\rho)$ over the plasma cross section is sufficiently weak. Defining the normalized radial variable

$$x=\rho/a\,, \tag{61}$$

then $xE'(x)/E\equiv\lambda_e$ is assumed to be $O(a/R_m)$. This ordering is valid for $\beta_p\lesssim 1$. The required metric coefficients become

$$\begin{aligned}\sqrt{g}=Aa^2E(x)x\Big[&\left(1-\frac{x}{A}\cos\theta-\frac{S(x)}{A}\right)[1+S'(x)\cos\theta]\\&+\lambda_e(x)\sin^2\theta-\frac{x\lambda_e(x)}{A}\sin^2\theta\cos\theta\\&-\frac{S(x)\lambda_e(x)}{A}\sin^2\theta+O(A^{-3})\Big]\,,\end{aligned} \tag{62}$$

$$\begin{aligned}\langle\sqrt{g}\rangle=Aa^2E(x)x\Big(&1-\frac{S(x)}{A}-\frac{1}{2}\frac{xS'(x)}{A}\\&+\frac{1}{2}\lambda_e(x)-\frac{1}{2}\frac{S(x)\lambda_e(x)}{A}+O(A^{-3})\Big)\end{aligned} \tag{63}$$

$$\begin{aligned}\left\langle\frac{\sqrt{g}}{g_{\phi\phi}}\right\rangle=\frac{E(x)x}{A}\Big(&1+\frac{S(x)}{A}+\frac{1}{2}\frac{xS'(x)}{A}+\frac{\lambda_e(x)}{2}+\frac{x^2}{2A^2}\\&+\frac{S^2(x)}{A^2}+\frac{xSS'(x)}{A^2}+\frac{1}{2}\frac{S(x)\lambda_e(x)}{A}+O(A^{-3})\Big)\,,\end{aligned} \tag{64}$$

$$\begin{aligned}\left\langle\frac{g_{\theta\theta}}{\sqrt{g}}\right\rangle=\frac{xE_a(x)}{AE(x)\delta(x)}\Big(&1-\frac{x\eta(x)}{2A}+\frac{S(x)}{A}-\frac{\lambda_e(x)}{2}\frac{3E_a-E^2}{E^2+\delta}\\&+\frac{1}{2}\frac{x^2\nu(x)}{A^2}+\frac{S^2(x)}{A^2}+\frac{x\lambda_e(x)}{2A}\frac{\xi(x)}{1+\delta(x)}+\frac{\lambda_e^2(x)}{2E_a(x)}\frac{5E_a-2E^2}{(1+\delta)^2}\\&-\frac{S(x)\lambda_e(x)}{2A}\frac{3E_a-E^2}{E^2+\delta}-\frac{xS(x)\eta(x)}{A^2}+O(A^{-3})\Big)\,,\end{aligned} \tag{65}$$

where

$$A=R_m/a\,, \tag{66}$$

$$S(x)=\Delta(\rho)/a\,, \tag{67}$$

$$\delta(x)=[1-S'^2(x)]^{1/2}\,, \tag{68}$$

$$E_a(x)=[E^2(x)+\delta(x)]/[1+\delta(x)]\,, \tag{69}$$

$$\xi(x)=2S'(x)/[1+\delta(x)]\,, \tag{70}$$

$$\eta(x)=\{[E^2(x)+E_a(x)]/2E_a(x)\}\xi(x)\,, \tag{71}$$

$$\nu(x)=[E^2(x)+E_a(x)]/[E^2(x)+\delta(x)]\,. \tag{72}$$

The moment equations (59) and (60) that determine the shift and ellipticity can now, in principle, be explicitly written as second-order ordinary differential equations. These equations are still quite complex. To obtain some analytic insight into the behavior of the shift and ellipticity, these equations may be linearized for the case of the small shift $S(x) \sim A^{-1}$, which pertains for low beta plasmas or near the magnetic axis. Assuming that E is approximately uniform, Eq. (59) becomes

$$(3E^2+1)\frac{d}{dx}[\hat{I}^2(x)S'(x)] - (3E^2+1)\hat{I}^2(x)\frac{S'(x)}{x}$$

$$= -(1/A)[2\beta_{p0}(E^2+1)^2x^3\hat{p}'(x) - 2(E^2+1)\hat{I}^2(x)$$

$$-(E^2-1)x\hat{I}'(x)\hat{I}(x)], \tag{73}$$

where

$$\hat{I}(x) = I(x)/I_0, \tag{74}$$

$$\hat{p}(x) = p(x)/p_0, \tag{75}$$

and

$$\beta_{p0} = \pi c^2 a^2 p_0 / I_0^2. \tag{76}$$

Integrating Eq. (73) yields

$$S(x) = \frac{1}{A}\int_0^x u[1+\Lambda(u)]du, \tag{77}$$

where

$$\Lambda(x) = \frac{2(E^2+1)}{(3E^2+1)}\frac{8\pi[\bar{p}(x)-p(x)]}{\tilde{B}_p^2(x)} + \frac{1}{2}\tilde{l}_i(x) + \frac{1}{2}\frac{E^2-1}{3E^2+1} - 1, \tag{78}$$

$$\bar{p}(x) = \frac{2}{x^2}\int_0^x up(u)du, \tag{79}$$

$$\tilde{l}_i(x) = \frac{4(E^2+1)}{(3E^2+1)}\frac{1}{x^2\tilde{B}_p^2(x)}\int_0^x u\tilde{B}_p^2(u)du, \tag{80}$$

$$\tilde{B}_p(x) = \frac{2I_0}{ca}\frac{\hat{I}(x)}{x\kappa}, \tag{81}$$

$$\kappa = [(E^2+1)/2]^{1/2}. \tag{82}$$

This analytic solution is similar in form to the Shafranov shift formula,[7] but it is a generalization to account for ellipticity. For an approximately uniform current density profile $\hat{I}(x) = x^2$ and a parabolic pressure profile $\hat{p}(x) = 1 - x^2$, the shift $S(x)$ is

$$S(x) = \frac{x^2}{2A}\left(\frac{2(E^2+1)}{3E^2+1}\bar{\beta}_p + \frac{1}{4} + \frac{E^2-1}{4(3E^2+1)}\right), \tag{83}$$

where

$$\bar{\beta}_p = [(E^2+1)/2]\beta_{p0}. \tag{84}$$

Equation (83) shows that for the same finite value of $\bar{\beta}_p$, plasma radius a, and aspect ratio A, the shift is smaller for a more elongated plasma. The expression for $S(x)$ in Eq. (83) is graphed in Fig. 2 for several values of the ellipticity as a function of $\bar{\beta}_p$. For comparison, the numerical solution of the moment equation (59) is also shown. For $\bar{\beta}_p \lesssim 1$, the linearized formula [Eq. (83)] appears to be adequate. When the current density is nonuniform, the dependence of the shift $S(x)$ on x is no longer parabolic. For example, consider the case $\hat{I}(x) = x^2(2-x^2)$, which corresponds to a nearly parabolic current density distribution. Taking $\hat{p}(x) = 1 - x^2$, we find that the shift is

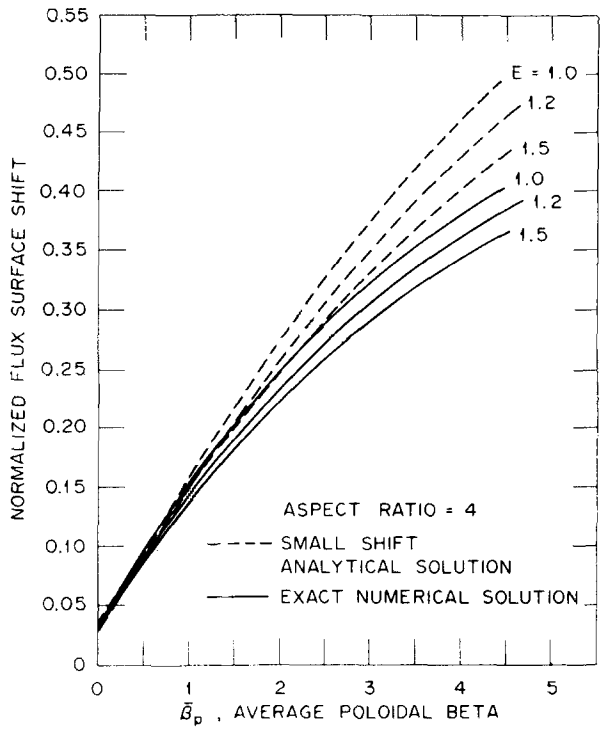

FIG. 2. Comparison of the shift calculated analytically with the exact numerical solution.

$$S(x) = \frac{1}{A}\left(\frac{(3E^2-1)}{8(3E^2+1)}x^2 + \frac{(E^2+1)}{6(3E^2+1)}\ln\frac{2}{2-x^2}\right.$$

$$\left. + \frac{(E^2+1)(6\bar{\beta}_p+1)}{12(3E^2+1)(2-x^2)}x^2\right). \tag{85}$$

Equations (83) and (85) show that for the same $\bar{\beta}_p$ the shift is greater for a more uniform current density distribution.

If there is a vacuum region between the plasma surface at $\rho = a$ and an ideally conducting wall at the boundary $\rho = b$, the shift of the plasma with respect to the wall $|\Delta(a) - \Delta(b)|$ can be obtained by matching the solution of Eq. (73) in the vacuum region, where $p'(\rho) = 0$ and $I'(\rho) = 0$, to the solution in the region inside the plasma. For example, consider the case $E = 1$. Then, for $a \leq \rho \leq b$,

$$\rho\Delta''(\rho) - \Delta'(\rho) = \rho/R_m; \tag{86}$$

integrating this equation yields

$$\Delta(\rho) = c_1 + c_2\rho^2 + (\rho^2/2R_m)\ln(\rho/a). \tag{87}$$

The constants c_1 and c_2 are determined by matching $\Delta(\rho)$ and $\Delta'(\rho)$ at $\rho = a$ to the solution inside the plasma. For the case $E = 1$, $\Delta'(\rho)$ for $\rho < a$ is given by Eq. (77) as

$$\Delta'(\rho) = \frac{\rho}{R_m}\left(\frac{8\pi[\bar{p}(\rho)-p(\rho)]}{\tilde{B}_p^2(\rho)} + \frac{\tilde{l}_i(\rho)}{2}\right). \tag{88}$$

Matching the solutions yields the shift[7] of the plasma surface at $\rho = a$ with respect to the wall at $\rho = b$:

$$|\Delta(a) - \Delta(b)| = \frac{b^2}{2R_m}\left[\ln\frac{b}{a} + \left(1 - \frac{a^2}{b^2}\right)\left(\frac{8\pi\bar{p}(a)}{\tilde{B}_p^2(a)} + \frac{\tilde{l}_i(a)}{2} - \frac{1}{2}\right)\right]. \tag{89}$$

Now, consider the ρ dependence of the ellipticity near the magnetic axis. Writing

$$E(x) = E_m + e(x) \tag{90}$$

and linearizing Eq. (60) for $e(x)/E_m \ll 1$ yields

$$\frac{E_m^4+6E_m^2+1}{16E_m(E_m^2+1)}e''(x)+\left(\frac{(3E_m^4+10E_m^2+3)}{16E_m(E_m^2+1)}\frac{\hat{I}'(x)}{\hat{I}(x)}\right.$$

$$\left.-\frac{1}{x}\frac{5E_m^4-10E_m^2+3}{16E_m(E_m^2+1)}\right)e'(x)+\left(\frac{x\hat{I}'(x)}{2\hat{I}(x)}-1\right)\frac{E_m e(x)}{x^2}$$

$$=\frac{2\beta_{p0}x^3\hat{p}'(x)}{A\hat{I}^2(x)}\left(\frac{E_m^2+1}{2}\frac{S(x)}{x^2}+\frac{(E_m^2+1)^2}{16x}S'(x)\right)$$

$$-\frac{S''(x)(5E_m^4-1)}{16A(E_m^2+1)}+\frac{S(x)(2E_m^4+3E_m^2-1)}{2Ax^2(E_m^2+1)}$$

$$-\frac{S'(x)(7E_m^4-12E_m^2+1)}{16Ax(E_m^2+1)}+\frac{E_m^2-1}{2x^2}\left(\frac{x\hat{I}'(x)}{2\hat{I}(x)}-1\right)$$

$$-\frac{x\hat{I}'(x)}{\hat{I}(x)}\left(\frac{S'(x)(11E_m^4+2E_m^2-5)}{16Ax(E_m^2+1)}+\frac{S(x)(2E_m^4-E_m^2-1)}{4Ax^2(E_m^2+1)}\right). \tag{91}$$

For the case $\hat{I}(x)=x^2$, which corresponds to an approximately uniform current density distribution, the coefficient of $e(x)$ vanishes. Assuming that the shift $S(x)$ has a parabolic profile $S(x)=S_m x^2$, Eq. (91) can be integrated for $E(x)$:

$$E(x) = E_m - E_1 x^2, \tag{92}$$

where

$$E_1 = \frac{S_m E_m}{A}\left(\frac{2\beta_{p0}(E_m^2+1)(E_m^4+6E_m^2+5)-(17E_m^4-12E_m^2-5)}{E_m^4+18E_m^2+5}\right). \tag{93}$$

For $E_m=1$, this reduces to

$$E(x) = 1-(2\bar{\beta}_p/A)S_m x^2. \tag{94}$$

V. NUMERICAL SOLUTIONS TO THE MOMENT EQUATIONS

A. Boundary conditions

In general, the set of second-order ordinary differential equations (29) and (30) that describe $R_n(\rho)$, $Z_n(\rho)$ or (35)–(38) that describe $E(\rho), R_n(\rho)$ must be solved numerically. Each moment equation must be supplemented with two boundary conditions. At the boundary $\rho = a$, the specification of the shape of the outermost flux surface provides one of the two boundary conditions:

$$R_n(a) = R_{na};\quad n=0,\ \ldots\ , \tag{95}$$

$$Z_n(a) = Z_{na};\quad n=1,\ \ldots\ , \tag{96}$$

or

$$R_n(a) = R_{na};\ n=0,\ldots\ , \tag{97}$$

$$E(a) = E_a. \tag{98}$$

To find the remaining boundary conditions, the condition is imposed that near the magnetic axis $\rho=0$ the flux surface geometry should have the representation given in Eqs. (44) and (45). Note that the amplitude of the first harmonic of R is chosen as the flux surface label ρ. Since both the amplitudes of the high harmonics R_n, Z_n $(n\geq 2)$ and their derivatives R_n', Z_n' vanish at the magnetic axis, $\rho=0$ is a critical point of the ordinary differential equations describing the amplitude functions. This asymptotic behavior is treated numerically by contracting the solution space in ρ from $(0,a)$ to (δ_0, a), where δ_0 is a small positive number. Then, the results of the previous section are used to write

$$R_0(\delta_0) = R_m + \lambda_1\delta_0^2, \tag{99}$$

$$R_n(\delta_0) = R_{n0}\delta_0^n;\quad n=2,\ \ldots\ , \tag{100}$$

$$Z_n(\delta_0) = Z_{n0}\delta_0^n;\quad n=1,\ \ldots\ , \tag{101}$$

$$E(\delta_0) = E_m + \lambda_2\delta_0^2, \tag{102}$$

where λ_1 and λ_2 are arbitrary, small constants. The solutions obtained using these boundary conditions are insensitive to the exact values of λ_1 and λ_2. The values of R_m, E_m, R_{n0}, and Z_{n0} are determined by the shape of the outermost flux surface through numerical iteration. Finally, if $p(\psi)$ and $F(\psi)$ are used as the driving functions instead of $p(\rho)$ and $I(\rho)$, the boundary conditions for $\psi(\rho)$ are

$$\psi(\delta_0) = \psi_m - \frac{8\pi^3E_m^2}{E_m^2+1}\left(R_m^2\frac{\partial p(0)}{\partial\psi}+\frac{1}{2\pi c^2}\frac{\partial F^2(0)}{\partial\psi}\right)\delta_0^2, \tag{103}$$

and

$$\psi(a) = \psi_a. \tag{104}$$

B. Numerical method

The moment equations (29) and (30) or (35)–(38) may be rewritten as a system of first-order differential equations of the form

$$\mathbf{u}' = \mathbf{f}(x,\mathbf{u}), \tag{105}$$

where the prime denotes differentiation with respect to x, and u is the vector comprised of the Fourier amplitudes of the inverse expansion and their first derivatives. The vector function f is an appropriate rearrangement of the moment equations. Equation (105) is then posed as a parameter estimation problem[8] by rewriting the appropriate boundary conditions given by Eqs. (95)–(104) in the form

$$\phi(x_l, x_r, \alpha, \mathbf{u}) = 0. \tag{106}$$

The subscripts l and r refer to the left and right boundaries in x located at $x_l=\delta_0/a$ and $x_r=1$, respectively, and $\phi=(\phi_{1l},\phi_{1l}',\phi_{2l},\phi_{2l}',\ldots,\phi_{1r},\phi_{1r}',\phi_{2r},\phi_{2r}',\cdots)$, where

$$\phi_{nl} = u_n(x_l) - u_{nl}(x_l, \alpha_{nl}), \tag{107}$$

and

$$\phi_{nr} = u_n(x_r) - u_{nr}(x_r, \alpha_{nr}). \tag{108}$$

For $u_n=R_n$, $u_{nl}=\alpha_{nl}(\delta_0/a)^n$ $(n\geq 2)$, or $u_{1l}=\alpha_{1l}-\lambda_1(\delta_0/a)^2$, where $\alpha_{nl}=R_{n0}a^n$ $(n\neq 1)$ and $\alpha_{1l}=R_m$ are the asymptotic expansion coefficients given in Eqs. (99) and (100). Also, $u_{nr}=R_{na}$ $(n\neq 1)$, and $u_{1r}=R_{0a}$. For $u_n=R_n'$, $u_{nl}=n\alpha_{nl}(\delta_0/a)^{n-1}$ $(n\neq 1)$ or $u_{1l}=2\lambda_1(\delta_0/a)$, and $u_{nr}=\alpha_{nr}$. (Similar expressions pertain for $u_n=Z_n$, Z_n', or E.) The constants α_{nl} and α_{nr} are unknown parameters to be determined along with the solution u.

The set of nonlinear coupled equations (105) and (106) are solved using a shooting technique.[8] The system of equations is integrated using a Runge–Kutta–Merson method and iterated using a modified Newton's method.

C. Comparison with exact two-dimensional equilibria

In order to demonstrate the capability of the moment method to accurately describe equilibria, a detailed comparison of the moment solutions with the more exact two-dimensional equilibria will now be presented for several values of the beta representative of current or anticipated tokamaks.

The exact two-dimensional flux surface geometry is obtained using the fixed boundary code RSTEQ,[9] which has been modified to use a Fourier series expansion of (R, Z) to specify the plasma boundary. The code uses an iterative, successive over-relaxation technique to solve the Grad-Shafranov equation (3) while simultaneously fixing

$$q(\psi) = -\frac{F(\psi)V'(\psi)}{\pi c}\left\langle \frac{1}{R^2} \right\rangle_f \tag{109}$$

(i.e., a flux conserving tokamak). The profiles $p(\psi)$ and $q(\psi)$ are specified as inputs to this two-dimensional equilibrium solver.

For comparison, two representative geometries are considered; (1) an ISX-B equilibrium of intermediate size and (2) an ETF/INTOR equilibrium of reactor size. The parameters for these cases are given in Table I. The outermost flux surface for either example is taken to have the form

$$R = R_{0a} - a\cos\theta + R_{2a}\cos 2\theta\,, \tag{110}$$

$$Z = E_a(a\sin\theta + R_{2a}\sin 2\theta)\,. \tag{111}$$

The profiles $p(\rho)$ and $I(\rho)$ are specified as the driving functions for the moment equations and are assumed to have the functional forms

$$p(x) = p_0(1 - x^2)^{\alpha_p} + p_b\,, \tag{112}$$

$$I(x) = I_0\left[\left(1 + \frac{1}{\alpha_I}\right) - \frac{1}{\alpha_I}x^2\right]^{\alpha_I} x^2\,, \tag{113}$$

where $\alpha_p = 2.0$ and $\alpha_I = 0.5$ are chosen for the numerical computation. Using the Fourier representation in Eqs.

TABLE I. Equilibrium parameters for ISX-B and ETF/INTOR geometries.

	ISX-B	ETF/INTOR
R_{0a}	91.9 cm	529 cm
a	27.0 cm	130 cm
R_{2a}	1.1 cm	13 cm
E_a	1.1	1.6
B_{t0}	12.9 kG	52 kG
I_0	220 KA	6.0 MA
$\bar{\beta}_t$	4%	5.7%
$\bar{\beta}_p$	3.3	4.0

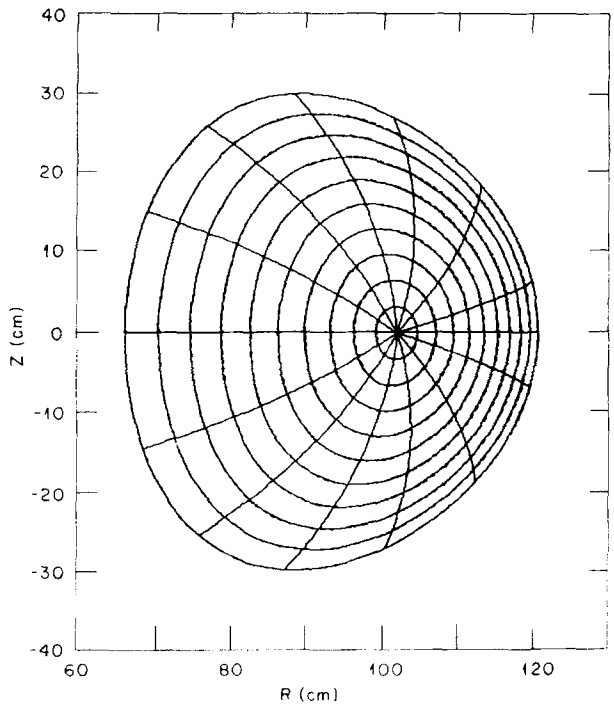

FIG. 3. Flux surface contours of an ISX-B equilibrium. The solid contours are computed from the moment method, and the dashed contours (which are barely distinguishable) are obtained from a two-dimensional solution of Eq. (3).

(33) and (34), the amplitudes $R_0(x)$, $R_2(x)$, and $E(x)$ are obtained numerically. From these solutions, $p(\psi)$ and $q(\psi)$ are constructed and are used as the inputs to the two-dimensional code RSTEQ.

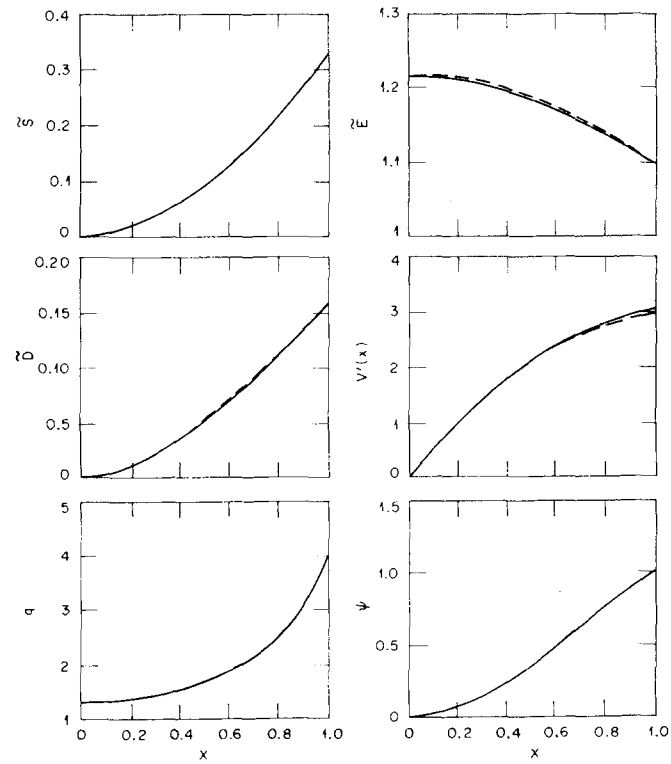

FIG. 4. Various ISX-B equilibrium profiles. Solid curves are obtained from the moment method and dashed curves from a two-dimensional solution of Eq. (3).

In Fig. 3, the flux surface contours (constant ρ contours) are shown for an ISX-B equilibrium. The dashed lines represent the two-dimensional calculation and the solid lines represent the moment calculation. Also shown in Fig. 3 are the contours of the constant poloidal angle θ, which are generally not orthogonal to the ρ contours. Figure 4 illustrates the normalized shift, elongation, and triangularity parameters of the flux surfaces $\tilde{S}(x)$, $\tilde{E}(x)$, and $\tilde{D}(x)$, respectively, for the two-dimensional and moment solutions. These equilibrium parameters correspond approximately to the variationally determined Fourier amplitudes $(R_m - R_0)/a$, Z_1/ρ, and R_2/a, but they are defined in a representation-independent form as

$$\tilde{S}(x) = (1/a)\{R_m - \tfrac{1}{2}[R(x,0) + R(x,\pi)]\}, \tag{114}$$

$$\tilde{E}(x) = |Z_{\max}(x)|/ax, \tag{115}$$

and

$$\tilde{D}(x) = (-1/a)\{R_{\max}(x) - \tfrac{1}{2}[R(x,0) + R(x,\pi)]\}, \tag{116}$$

where $R_{\max} = R(Z_{\max})$ and $(R_{\max}, Z_{\max})$ is the point of a flux surface at which $Z_\theta = 0$. Figure 4 also provides a comparison of the differential flux surface volume $V'(x)$, the safety factor $q(x)$, and the poloidal magnetic flux $\psi(x)$. Figure 5 compares $\tilde{J}(x), J_0[R(0)], I(x)$, and $p(x)$, where $\tilde{J}(x)$ is the flux surface averaged toroidal current density

$$\tilde{J}(x) = \langle J_\phi/R\rangle_f / \langle R^{-1}\rangle_f, \tag{117}$$

and $J_0 = J_\phi(\psi, 0)$ is the toroidal current density J_ϕ measured along the major radius R in the plane $Z = 0$ $(\theta = 0)$. Once again, the dashed lines represent the two-dimensional calculation, and the solid lines represent the moment calculation results. The same comparisons are shown in Figs. 6–8 for an ETF/INTOR equilibrium. In all cases, there is close agreement between the two-dimensional results and the moment method.

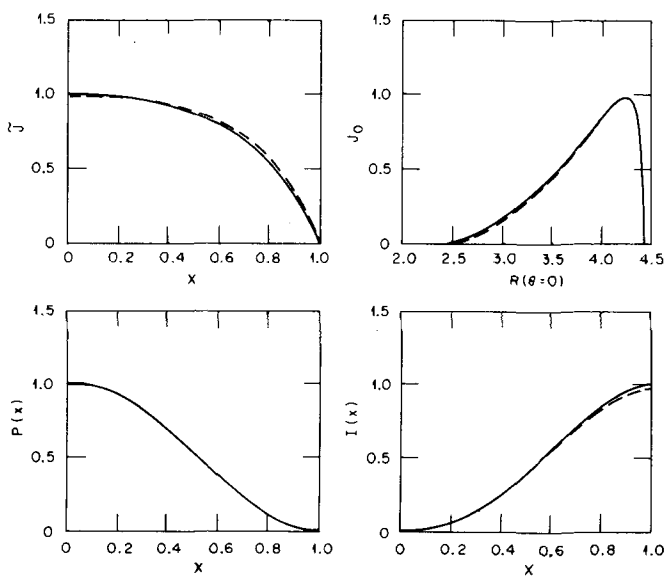

FIG. 5. Various ISX-B equilibrium profiles. Solid curves are obtained from the moment method and dashed curves from a two-dimensional solution of Eq. (3).

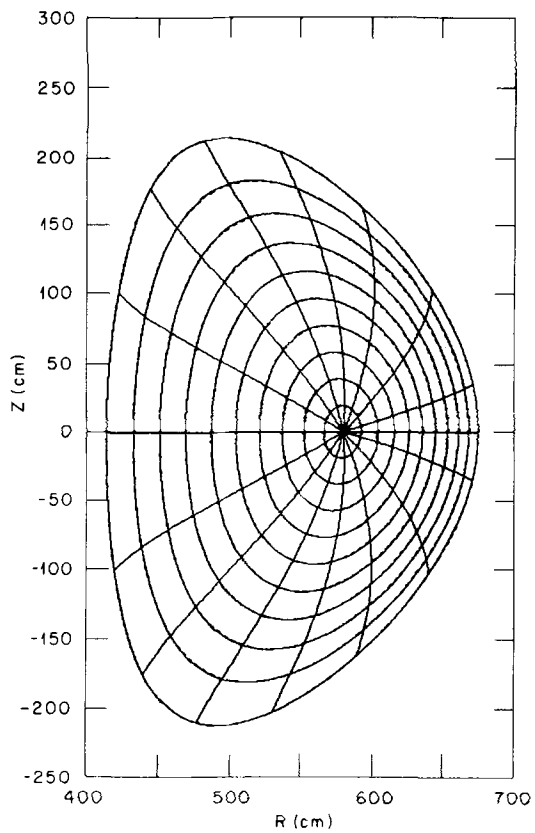

FIG. 6. Flux surface contours of an ETF/INTOR equilibrium. The solid contours are computed from the moment methods, and the dashed contours (which are barely distinguishable) are obtained from a two-dimensional solution of Eq. (3).

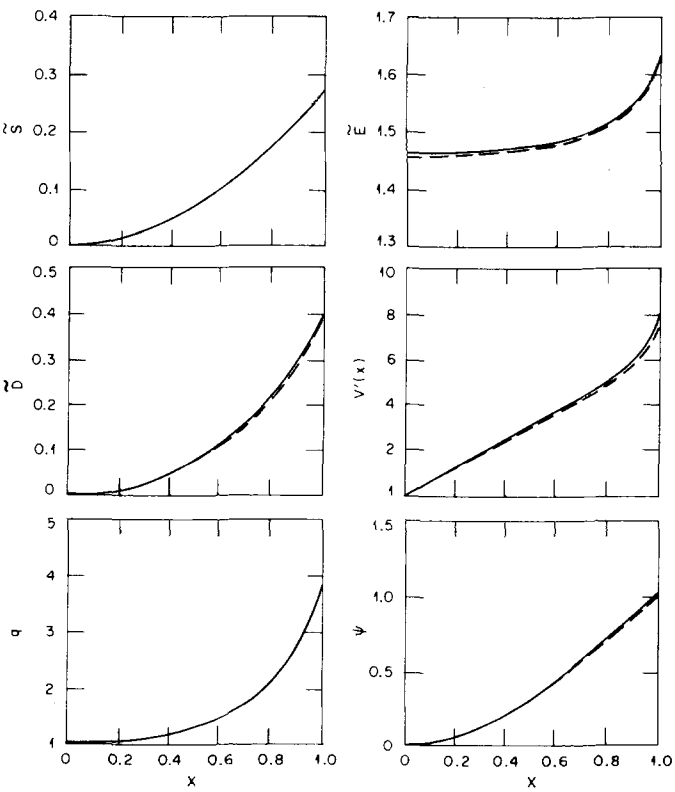

FIG. 7. Various ETF/INTOR equilibrium profiles. Solid curves are obtained from the moment method and dashed curves from a two-dimensional solution of Eq. (3).

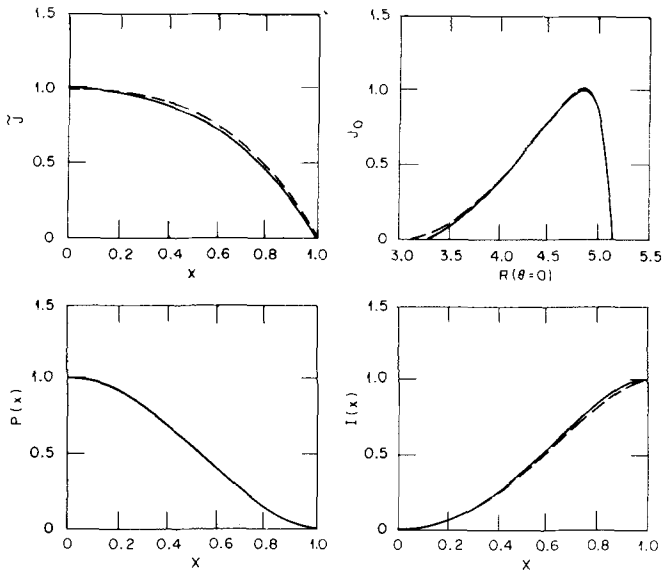

FIG. 8. Various ETF/INTOR equilibrium profiles. Solid curves are obtained from the moment method and dashed curves from a two-dimensional solution of Eq. (3).

D. Discussion

The amount of computer time required for the moment method depends on the number of amplitude functions being determined and on the relative error desired. A relative error specification of 10^{-3} generally yields sufficient accuracy, and the number of amplitude functions required is primarily determined by the shape of the outermost flux surface. For a given number of amplitude functions, a good choice of the poloidal angle θ to represent the outermost flux surface generally gives a better global result for the flux contours. Once a certain θ is chosen to represent the outermost flux surface, the variational principle will select the "optimum" θ, which makes the volume integral Q given in Eq. (11) stationary. For a D-shaped plasma boundary, three amplitude functions (R_0, E, R_2) usually suffice. For an elliptic boundary, two functions (R_0, E) are usually sufficient. A typical variational calculation with a relative error of 10^{-3} requires approximately 50–100 msec of CRAY time for two amplitude functions and approximately 150–250 msec of CRAY time for three amplitude functions. On the other hand, the same computation using the two-dimensional code RSTEQ , with a 40 $\times$35 mesh and a relative error of 10^{-3}, requires about 7–10 sec of CRAY time and significantly more storage space. Thus, the moment method is faster by at least a factor of 10 in computational speed while reproducing the same equilibrium with a degree of accuracy sufficient for many purposes.

The two equilibria considered in this section have also been computed using the homogeneous moment procedure.[5,6] As noted previously, the accuracy of this method is comparable to the variational method when a sufficient number of amplitude coefficients are retained in the inverse mapping. (In the cases considered, the shift, the ellipticity, and the triangularity must be calculated). However, the complexity of the higher-order homogeneous basis functions (which are required to compute the amplitudes of the higher Fourier harmonics for $n \geq 2$) makes this method slower in computational speed than the (self-adjoint) variational moment method. In the cases considered, it is slower by about 30%.

ACKNOWLEDGMENTS

The authors would like to thank D. J. Sigmar, H. K. Meier, W.A. Houlberg, and J.A. Holmes for useful discussions. H. Weitzner's encouragement throughout the development of this work, as well as his contributed Appendix, are also greatly appreciated.

This research was sponsored by the Office of Fusion Energy, U.S. Department of Energy, under contract W-7405-eng-26 with the Union Carbide Corporation.

APPENDIX

Harold Weitzner

Courant Institute of Mathematical Sciences
New York University
New York, New York 10012

The variational principle for axisymmetric magnetohydrodynamic equilibria derived in the main text employs parametric representations of flux surfaces which are of the form

$$R = \sum_{n=0}^{\infty} R_n(\psi) \cos n\theta ,$$
$$Z = \sum_{n=1}^{\infty} Z_n(\psi) \sin n\theta , \tag{A1}$$

where (R, Z) are the coordinates of a point in cylindrical coordinates. Such surfaces have reflection symmetry through the plane $Z = 0$. In this representation, ψ determines a given flux surface and θ is an arbitrary parameter which maps out the points on the surface. We assume that θ covers all values in the range $0 \leq \theta \leq 2\pi$. Of course, the representation in Eq. (A1) is not unique, since the substitution

$$\theta = \bar{\theta} + a \sin\bar{\theta}, \quad |a| < 1 ,$$

generates an equivalent representation of the same surfaces

$$R = \sum_{n=0}^{\infty} \bar{R}_n(\psi) \cos n\bar{\theta} ,$$
$$Z = \sum_{n=1}^{\infty} \bar{Z}_n(\psi) \sin n\bar{\theta} ,$$

$0 \leq \bar{\theta} \leq 2\pi$. It is the purpose of this appendix to justify two specific representations of flux surfaces which are frequently used.

Equation (A1) may be interpreted as the representation of a family of nested curves in the (R, Z) plane which are symmetric about the line $Z = 0$. Fixing the value of ψ selects the representation of just one symmetric curve in the (R, Z) plane. It therefore suffices to explore the possibility of representations of smooth, closed curves, symmetric about $Z = 0$ in the form

$$R = \sum_{n=0}^{\infty} R_n \cos n\theta , \tag{A2}$$

$$Z=\sum_{n=1}^{\infty} Z_n \sin n\theta .$$

It is clear that the representation of a family of surfaces in Eq. (A1) may be recovered from the representation of one curve in Eq. (A2) by allowing the constants R_n, Z_n to become functions of ψ and by considering R and Z as cylindrical coordinates.

Let Γ denote a smooth, closed curve in the (R,Z) plane and assume that Γ is symmetric about the line $Z=0$. Consider the plane of the complex variable $\zeta = \rho\exp(i\theta)$. Also, consider the complex variable $\xi = R + iZ$ and the curve Γ in the complex ξ plane. By the Riemann mapping theorem, there is a unique analytic function $F(\zeta)=\xi$ which maps the interior of the unit circle $|\zeta|<1$ onto the interior of the curve Γ and which satisfies

$$F(0)=R_0, \quad F'(0)>0, \tag{A3}$$

where R_0 is real and a point in the interior of Γ. Now, $F(\zeta)$ has a power series representation

$$F(\zeta)=\sum_{n=0}^{\infty} R_n \zeta^n . \tag{A4}$$

It is easy to verify that $[F(\zeta^*)]^*$ is an analytic function of ζ which maps the interior of $|\zeta|=1$ onto the interior of Γ and which satisfies Eq. (A3). (Here, the superscript asterisk denotes complex conjugation.) Hence, the uniqueness of F implies $[F(\zeta^*)]^* = F(\zeta)$, and thus the coefficients R_n in Eq. (A4) are real. Under fairly general conditions the image of $|\zeta|=1$ is Γ, so that if we set $\zeta=\exp(i\theta)$ in Eq. (A4) and separate real and imaginary parts, we find the representation of Γ

$$\begin{aligned} R &= R_0+\sum_{n=1}^{\infty} R_1 \cos n\theta , \\ Z &= \sum_{n=1}^{\infty} R_1 \sin n\theta . \end{aligned} \tag{A5}$$

Note that Eq. (A5) has only one set of constants (R_n), rather than two sets (R_n, Z_n) as does Eq. (A2). The representation in Eq. (A5) is uniquely determined once the one constant R_0 is given.

Another representation may be obtained by introducing the complex variable $\xi = R + iZ/E$, where E is an arbitrary real constant. The curve Γ in the (R,Z) plane has a image Γ' in the ξ plane. Consider the mapping of the interior of the unit circle in the ζ plane onto the exterior of the curve Γ' in the ξ plane such that $\zeta=0$ maps to infinity in the ξ plane and the positive real axis near $\zeta=0$ maps to the positive real axis near infinity in the ξ plane. Again, such a mapping is unique. Let $\xi = F(\zeta)$ be the mapping. Then, $F(\zeta)$ has the Laurent expansion

$$F(\zeta)=\frac{R_{-1}}{\zeta}+\sum_{n=0}^{\infty} R_n \zeta^n . \tag{A6}$$

Since $[F(\zeta^*)]^*$ is also such a conformal mapping, the uniqueness theorem implies that all the coefficients R_n in Eq. (A6) are real. Under general conditions, the unit circle $|\zeta|=1$ maps onto the curve Γ'. Setting $\zeta = \exp(i\theta)$ in Eq. (A6) and separating real and imaginary parts yields a representation of Γ.

$$\begin{aligned} R &= R_0+(R_{-1}+R_{+1})\cos\theta+\sum_{n=2}^{\infty} R_n \cos n\theta , \\ Z &= E(-R_{-1}+R_{+1})\sin\theta+E\sum_{n=2}^{\infty} R_n \sin n\theta , \end{aligned} \tag{A7}$$

All the coefficients R_n in Eq. (A7) are specified once E is given. We next show there are values of E (we conjecture exactly one value) such that $R_{+1}=0$. When $R_{+1}=0$, Eq. (A7) is the representation used in Ref. 1 to give particularly simple descriptions of the ellipticity of flux surfaces.

As $E\to+\infty$, the curve Γ' approximates a slit on the real axis in the ξ plane. The mapping from $|\zeta|<1$ onto the exterior of a slit on the real axis is

$$F(\zeta)=R_0+A(\zeta+1/\zeta), \tag{A8}$$

where $A>0$. The mapping of $|\zeta|<1$ onto the exterior of Γ must be approximately Eq. (A8), from which we conclude that for E large enough $R_{+1}>0$. As $E\to 0^+$, we see that the curve Γ' approximates a slit on the imaginary axis in the ξ plane. In this case the map is approximately

$$F(\zeta)=R_0+A(1/\zeta-\zeta),$$

$A>0$, for which $R_{+1}<0$. Thus, for E sufficiently small $R_{+1}<0$. Since R_{+1} is a continuous function of E we conclude that there must be values of E for which $R_{+1}\equiv 0$. Thus, a representation

$$\begin{aligned} R &= R_0+R_{-1}\cos\theta+\sum_{n=2}^{\infty} R_n \cos n\theta , \\ Z &= -ER_{-1}\sin\theta+E\sum_{n=2}^{\infty} R_n \sin n\theta , \end{aligned} \tag{A9}$$

is always possible and the coefficients are essentially completely determined.

[1] H. K. Meier (private communication); H. K. Meier, S. P. Hirshman, D. J. Sigmar, and L. L. Lao, Oak Ridge National Laboratory Report ORNL/TM-7584 (1981).

[2] J. M. Greene, J. L. Johnson, and K. E. Weimer, Phys. Fluids **14**, 671 (1971).

[3] V. D. Hait, Fiz. Plazmy **6**, 871 (1980) [Sov. J. Plasma Phys. **6**, 476 (1980)].

[4] P. N. Vabishchevich, L. M. Degtyarev, and A. P. Favorskii, Fiz. Plazmy 4, 995 (1978) [Sov. J. Plasma Phys. 4, 554 (1978)].

[5] L. E. Zakharov and V. D. Shafranov, Kurchatov Institute Report IAE-3075 (1978).

[6] L. E. Zakharov and V. D. Shafranov, Zh. Tekh. Fiz. 43, 225 (1973) [Sov. Phys.-Tech. Phys. **18**, 151 (1973)].

[7] V. D. Shafranov, in *Reviews of Plasma Physics*, edited by M. A. Leontovich (Consultants Bureau, New York, 1970), Vol. 2, p. 130.

[8] I. Gladwell, University of Manchester Department of Mathematics Numerical Analysis Report 35 (1979); D02AGF, Numerical Algorithms Group Library (NAG), Downer's Grove, Ill.

[9] J. A. Holmes, Y-K. M. Peng, and S. J. Lynch, J. Comput. Phys. **36**, 35 (1980).